Fermionic interpretation of the quantum phase transition in XXZ magnets

Tao Yang,[1] Bangming Wang,[1] Peng Song,[1,2,*] Rui Wang,[1,2,†] and Baigeng Wang[1,2,‡]
[1]*National Laboratory of Solid State Microstructures and Department of Physics, Nanjing University, Nanjing 210093, China*
[2]*Collaborative Innovation Center for Advanced Microstructures, Nanjing 210093, China*

(Received 22 June 2022; revised 25 September 2022; accepted 18 October 2022; published 31 October 2022)

Quantum phase transitions in quantum magnets constitute an important field that has attracted great interests. Although a variety of analytic and numerical methods have been introduced in this direction, faithful fermionic descriptions are still desired because they can transform the spin models to a form tractable by conventional many-body techniques, yielding more transparent physical pictures. We generalize the Chern-Simons fermionization approach and apply it to the XXZ quantum magnets. After fermionzation, the Ising interaction of the XXZ spin model leads to a fermion-fermion interaction. We show that the additional fermion-fermion interaction generates an interesting phase transition between two fermionic ordered states, i.e., the Chern-Simons superconductor and the Chern-Simons exciton insulator. We also demonstrate that this transition in the fermionic language essentially describes the quantum phase transition between the planar and out-of-plane Néel orders in the spin picture. The fermionic mean-field theory further leads to a nonlinear σ model that describes the quantum phase transition, which is further supported by our density matrix renormalization group calculations in the original spin model. Our work introduces a fermionic interpretation of quantum phase transitions and advances the existing knowledge of quantum magnets.

DOI: 10.1103/PhysRevB.106.144438

I. INTRODUCTION

Quantum spin systems host a rich variety of strongly correlated phenomena, ranging from quantum magnetism [1,2] to quantum spin liquids (QSLs) [3–7], and they are also related to many exotic phases, such as the quantum Hall effect [8–11] and high-T_c superconductivity [12,13]. One interesting direction under extensive study is the quantum phase transitions (QPTs) in low-dimensional quantum magnets [14]. In these systems, the strong quantum fluctuations at the critical point lead to abrupt changes of the many-body ground state, crossing either a continuous or a first-order transition point.

In quantum magnets, understanding how the many-body ground state evolves during the quantum phase transition is a major theoretical challenge. To this end, a number of efficient numerical methods, such as density matrix renormalization group (DMRG) [15,16] and tensor renormalization group [17], have been developed. On the theoretical side, analytic approaches mainly focus on the effective field theories capturing the low-energy and long-wave properties of the systems. Although the conventional mean-field approaches can be applied to study the microscopic models, they usually bring about approximations with bias, thus would fail in characterizing the nature of the quantum phase transitions. Hence, to fully understand the quantum phases and transitions in quantum magnets, it is desirable to find out more mean-field descriptions beyond the conventional scope, which may produce new understandings towards QPTs when combined with numerical simulations.

A well-known mean-field approach to quantum spin systems is based on the parton construction [18–20]. For example, the spin-$\frac{1}{2}$ operators in spin-half systems are fermionized or bosonized with an additional constraint condition of single occupation on each site. These constructions have the advantage in formulating topological ordered states such as QSLs because they inherently introduce the gauge degrees of freedom that are absent in the spin models but are essential in QSLs [21,22]. However, because of the local constraint condition, the emergent gauge field is indispensable and strongly coupled to the partons. Thus, Gutzwiller projection to the single-site occupation subspace is required, which is a complication that obscures the nature of the physical spin wave function.

Another interesting mean-field approach based on the flux attachment [23–29] originally proposed in the study of fractional quantum Hall states [9] has been applied to frustrated quantum magnets. Instead of representing the spin operators by spinful fermions or bosons with constraint, spinless Chern-Simons (CS) fermions are introduced, which are attached to the U(1) CS gauge field [30,31]. Such a representation is free from the single occupation constraint and has been successfully generalized to investigate magnetically ordered states [32,33], certain QSLs [34], and the transitions between them [35]. It should be emphasized that, in previous studies, the XY models were intentionally considered [33,35–37] because they can be cast into a simple form under the CS fermionization, i.e., a fermionic theory coupled to U(1) gauge field. However, in realistic magnetic materials, the XY interactions cannot describe the actual spin-spin interactions. Instead, it is

*songpengphysics@nju.edu.cn
†rwang89@nju.edu.cn
‡bgwang@nju.edu.cn

the Heisenberg or XXZ interaction with an easy axis or an easy plane that usually takes place. Therefore, to make the CS fermionization approach truly applicable to realistic magnetic materials, its generalizations to the XXZ quantum magnets are highly desired. Unfortunately, such generalizations are still lacking.

Compared to the XY models, the XXZ quantum magnets display richer quantum phenomena, including the QPTs between different ordered states. Hence, some unanswered but crucial questions arise, namely, how to describe these ordered states using the CS mean-field theory, and whether the CS representation will bring about any different understandings of the QPTs.

In this work, we generalize the CS mean-field theory to study the antiferromagnetic (AFM) XXZ quantum magnet, and obtain results absent in previous works. We fully explore the physical effects induced by the Ising interaction and the anisotropy. Using DMRG simulation, we first show that there occurs a QPT from the in-plane to the out-of-plane Néel orders after the Ising interaction is tuned to be larger than the XY interaction. Then, we formulate the mean-field theory of the XXZ magnet based on the CS fermionization. In the fermionic picture, we observe an interesting transition between two effective mean-field orders, i.e., the CS superconductor state and the CS exciton insulator. The CS superconductor state is an effective state formed by pairing of the spinless CS fermions, which has been known to describe the planar Néel AFM [32,33,36,37]. In comparison, the CS exciton insulator is formed by the pairing of electron and hole states of the CS fermions. We clearly show that this phase exhibits staggered fermion density on different sublattices, which is translated into the spin language as the out-of-plane Néel order. Hence, the DMRG results on the QPT, which show a transition between in-plane and out-of-plane magnetization, acquire a unique fermionic interpretation in the CS representation. Furthermore, we show that the CS mean-field theory provides a natural starting point to construct an effective field theory that describes the QPT. For the studied XXZ model, we arrive at an O(3) nonlinear σ model that describes the critical regime, which is further supported by DMRG calculations. The fermionic perspective on quantum magnetism, although derived from XXZ quantum magnets, is generalizable and may find applications in more complicated systems with various QPTs.

II. THE QPT FROM IN-PLANE TO OUT-OF-PLANE NÉEL AFM ORDER

We start from the AFM spin-$\frac{1}{2}$ XXZ model given by

$$H_{\mathrm{XXZ}} = \sum_{\langle i,j\rangle} J_x\left(S_i^x S_j^x + S_i^y S_j^y\right) + J_z S_i^z S_j^z, \tag{1}$$

where J_x and J_z denote the XY and the Ising interactions, respectively. This model has been fully investigated, which is known to support the AFM magnetic orders on nonfrustrated lattices at zero temperature. Here, we will demonstrate how to solve the model using the CS fermionic mean-field theory and aim to uncover the underlying physics exclusive to the CS representation. Since our main interest lies in QPT between the ordered states, we assume that Eq. (1) is defined on a bipartite lattice. We take the honeycomb lattice as an example, and generalizations to other bipartite lattices are straightforward.

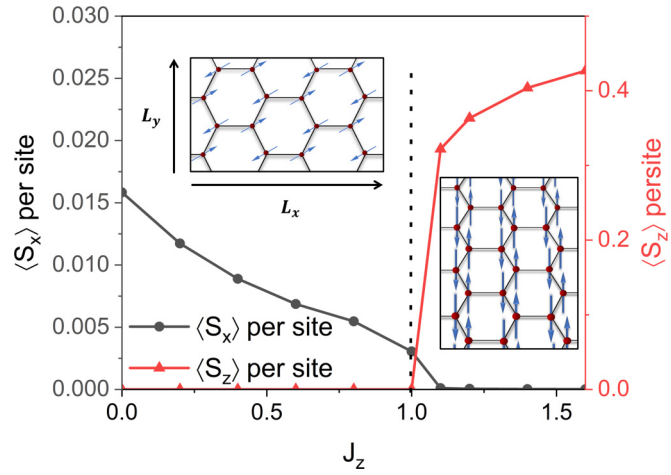

FIG. 1. The DMRG results of the magnetic orders on honeycomb lattice with $L_y = 8$ and $L_x = 14$. The pinning field $\beta = 10^{-4}$ is introduced along the x direction in the calculations. We defined the staggered magnetization $\langle S_{x/z}\rangle$ to be $\langle S_{x/z}\rangle = \langle S_{x/z,A}\rangle = -\langle S_{x/z,B}\rangle$. The components of the magnetization changes from the case where $\langle S_x\rangle$ dominates to the opposite case where $\langle S_z\rangle$ dominates as the strength of the Ising term J_z increases. There is a phase transition at $J_z/J_x = 1$. At the critical point, the O(3) symmetry seems to be violated since $\langle S_x\rangle \neq 0$ and $\langle S_z\rangle = 0$. However, this is a numerical artifact generated by the pinning field β. A close investigation of the O(3) symmetry at the critical point will be presented below. The insets show the in-plane and out-of-plane Néel AFM states.

We set $J_x = 1$ as the energy unit and regard J_z/J_x as the tuning parameter. For $J_z/J_x = 0$, the model is reduced to the XY model, where the ground state at zero temperature is the planar Néel AFM that spontaneously breaks the planar U(1) symmetry. The magnetization of this phase is opposite on the neighboring two sublattices and is completely in plane. With increasing J_z/J_x from zero, the XY plane remains as the easy plane for $J_z/J_x < 1$, and one expects that the system will stay as the planar Néel AFM state. For $J_z/J_x > 1$, the Ising term dominates and generates an easy axis. In this case, the out-of plane magnetization tends to form along the z direction, with opposite $\langle S^z\rangle$ for the different neighboring sublattices. Accordingly, the SU(2) symmetric point $J_z/J_x = 1$ is a critical point of the QPT. By crossing this critical point, a QPT is expected to take place separating the in-plane and the out-of-plane AFM Néel states.

We first perform a DMRG simulation with respect to Eq. (1) on cylinders of different sizes. The periodic and open boundary conditions are enforced along the x and y directions, respectively. To simulate the effect of spontaneous symmetry breaking on a finite lattice, we assign a very weak pinning field on the open boundary and calculate the magnitude of spin expectations in the bulk, i.e., $\langle S^x\rangle$ and $\langle S^z\rangle$ with varying J_z/J_x. As shown in Fig. 1, we observe that $\langle S^x\rangle$ is generally finite while $\langle S^z\rangle = 0$ for $J_z/J_x \lesssim 1$, displaying an in-plane Néel AFM as indicated by the inset of Fig. 1. For $J_z/J_x \gtrsim 1$, $\langle S^z\rangle$ grows with a vanishing $\langle S^x\rangle$, clearly suggesting an out-of-plane Néel AFM order as shown by the inset to Fig. 1.

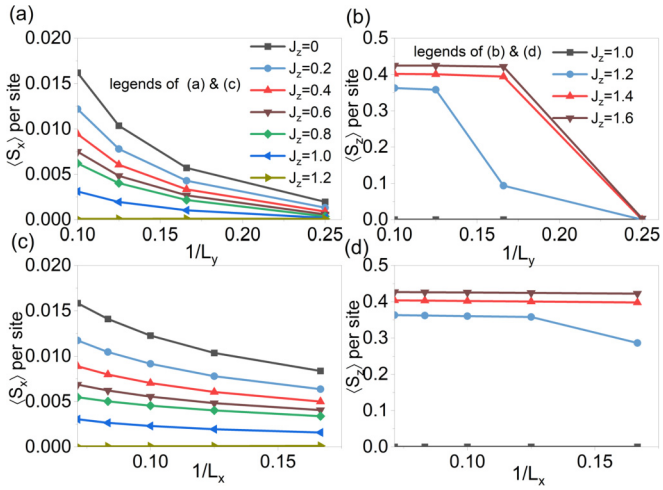

FIG. 2. The magnetization is calculated with varying the system size. $\langle S^x\rangle$ and $\langle S^z\rangle$ are plotted against both the length (L_x) and the circumference (L_y) of the cylinder. In (a) and (b), L_x is fixed to be $L_x = 8$, and in (c) and (d) $L_y = 8$.

The spin expectations with varying system sizes are calculated and shown by Fig. 2. The calculated $\langle S^x\rangle$ with varying L_y and L_x is shown in Figs. 2(a) and 2(c) for different J_z/J_x. It is clearly shown that for $J_z/J_x \lesssim 1$, $\langle S^x\rangle$ grows with increasing system size, while it always remains at zero for $J_z/J_x \gtrsim 1$, regardless of the system size. This verifies the spontaneous symmetry breaking of the planar U(1) symmetry in the thermodynamic limit. Figures 2(b) and 2(d) show the calculated $\langle S^z\rangle$ with varying L_y and L_x, respectively. $\langle S^z\rangle$ remains zero up to $J_z/J_x \simeq 1$ and takes a nonzero value for $J_z/J_x > 1$. Besides, for $J_z/J_x > 1$, $\langle S^z\rangle$ is found to be nearly saturated as we enlarge the system size beyond $L_y \geqslant 8$. This confirms the spontaneous formation of the out-of-plane Néel AFM in this regime.

The DMRG calculation suggests the emergence of a QPT from the planar to the out-of-plane Néel AFM state. Although the physical mechanism is clear in the spin picture, we emphasize that it is of importance to consider whether the observed QPT as well as the magnetic orders can be reinterpreted using fermionic mean-field theories. The latter not only brings about different understandings to QPTs, but also provides us with a useful approach to study QSLs when the frustration is further turned on [34,35].

III. CHERN-SIMONS FERMIONIZATION OF THE QUANTUM XXZ MAGNET

In previous works, the CS fermionization has been applied to XY models. We first briefly revisit how to fermionize the quantum spin model. The spin-$\frac{1}{2}$ operators $S^{\pm}_{\mathbf{r}}$ on a lattice can be represented using spinless fermions attached to the string operator, i.e.,

$$S^{+}_{\mathbf{r}} = f^{\dagger}_{\mathbf{r}} U^{+}_{\mathbf{r}}, \quad S^{-}_{\mathbf{r}} = f_{\mathbf{r}} U^{-}_{\mathbf{r}}, \tag{2}$$

where $f_{\mathbf{r}}$ and $f^{\dagger}_{\mathbf{r}}$ denote the annihilation and creation operator for spinless fermions at site $\mathbf{r}$, and the string operator $U^{\pm}_{\mathbf{r}}$ is given by

$$U^{\pm}_{\mathbf{r}} = e^{\pm ie\sum_{\mathbf{r}\neq\mathbf{r}'} \arg(\mathbf{r}-\mathbf{r}')n_{\mathbf{r}'}}, \tag{3}$$

where e, the CS charge, is an odd integer, so that it reproduces the SU(2) algebra of spin operators. The phase factor here involves the sum of the fermion number operator $n_{\mathbf{r}'} = f^{\dagger}_{\mathbf{r}'} f_{\mathbf{r}'}$ with the weight $\arg(\mathbf{r}-\mathbf{r}')$. The latter denotes the angle of the vector $\mathbf{r}-\mathbf{r}'$. In addition, we note that Eqs. (2) and (3) also lead to $S^z_{\mathbf{r}} = f^{\dagger}_{\mathbf{r}} f_{\mathbf{r}} - \frac{1}{2}$.

When $J_z/J_x = 0$, the XY model can be readily mapped to a fermionic theory coupled to U(1) gauge field using Eqs. (2) and (3) [32,33,36]. To solve the fermionized model, we first treat the U(1) gauge field as static fluxes and minimize the fermion energy with respect to the fluxes. In this step, the half-filling condition is enforced since the possible ground state for the XXZ model should enjoy $\langle S^z_{\mathbf{r}}\rangle = 0$ in a magnetic unit cell, which corresponds to the half-filling condition $\langle f^{\dagger}_{\mathbf{r}} f_{\mathbf{r}}\rangle = \frac{1}{2}$. The above fermionization leads to the flux states that enjoy low-energy Dirac fermions. On the honeycomb lattice, the state is described by Dirac fermions with two Dirac valleys in momentum space [33]. The corresponding low-energy effective Hamiltonian is derived to be

$$H_0 = v_F \sum_{\mathbf{k}} (f^{(+)\dagger}_{\mathbf{k}} \mathbf{k}\cdot\boldsymbol{\sigma} f^{(+)}_{\mathbf{k}} - f^{(-)\dagger}_{\mathbf{k}} \mathbf{k}\cdot\boldsymbol{\sigma} f^{(-)}_{\mathbf{k}}), \tag{4}$$

where $\boldsymbol{\sigma}$ is the Pauli matrix denoting the sublattice degrees of freedom and $f^{(\pm)}_{\mathbf{k}} = [f^{(\pm)}_{\mathbf{k},A}, f^{(\pm)}_{\mathbf{k},B}]^{\mathrm{T}}$ is the annihilation operator of the CS fermions in the $\pm$ Dirac valley. $v_F = \sqrt{3}/2J_x a$, with a being the lattice constant of the honeycomb lattice.

The full low-energy physics is then described by restoring the gauge fluctuations of the Dirac fermions in Eq. (4). The U(1) CS gauge field induces the fermion-fermion interaction, i.e.,

$$H_{\mathrm{XY}} = \sum_{\mathbf{k},\mathbf{k}',\mathbf{q}} V^{\alpha\alpha'\beta'\beta}_{\mathbf{q}} f^{\dagger}_{\mathbf{k}\alpha} f^{\dagger}_{\mathbf{k}'+\mathbf{q}\alpha'} f_{\mathbf{k}'\beta'} f_{\mathbf{k}+\mathbf{q}\beta} \tag{5}$$

with the interaction vertex

$$V^{\alpha\alpha'\beta'\beta}_{\mathbf{q}} = -2\pi i e v_F \epsilon^{ij} \left(\sigma^i_{\alpha\beta}\delta_{\alpha'\beta'} + \sigma^{i\mathrm{T}}_{\alpha\beta}\delta_{\alpha'\beta'}\right) A^j_{\mathbf{q}}, \tag{6}$$

where α, β are the sublattice indices and $A^j_{\mathbf{q}} = q^j/|q|^2$.

The gauge-field-induced interaction has been carefully analyzed by Refs. [33,36], and is found to generate the CS superconductor state with $p+ip$ pairing symmetry. The CS superconductor has been shown to be a good fermionic description of the planar Néel state [33,36]. In particular, these two states enjoy qualitatively the same collective excitations as well as the spin orders.

The XXZ model has a key distinction from the above results after fermionization, namely, an additional fermion-fermion interaction that arises from the Ising term. Inserting $S^z_{\mathbf{r}} = n_{\mathbf{r}} - \frac{1}{2}$, the nearest-neighbor Ising interaction is cast into

$$H_{\mathrm{Ising}} = 3J_z \sum_{\mathbf{r}} (f^{\dagger}_{A,\mathbf{r}} f_{A,\mathbf{r}} - 1/2)(f^{\dagger}_{B,\mathbf{r}} f_{B,\mathbf{r}} - 1/2), \tag{7}$$

where A and B are indices for the sublattices, and $f_{A,\mathbf{r}}/f_{B,\mathbf{r}}$ is the annihilation operator of the CS fermion at $\mathbf{r}$. This term describes the density-density interaction between the fermions on different sublattices, which is distinct in nature from the gauge-field-induced interaction, as its origin has nothing to

do with the CS gauge field. Therefore, two fermion-fermion interaction terms, Eqs. (5) and (7), emerge under CS fermionization for the quantum XXZ model. The interplay between these interactions remains unstudied. The natural question then arises that whether the CS fermion theory can faithfully describe the transition from the planar to the out-of-plane Néel order found in the original spin picture.

Before proceeding, we can further transform $H_{\rm Ising}$ into momentum space and make a projection to the low-energy window around the two Dirac valleys described by Eq. (4), leading to

$$\begin{aligned} H_{\rm Ising} = {} & 3J_z \sum_{\mathbf{k},\mathbf{k}',\mathbf{q},a} f^{(a)\dagger}_{A,\mathbf{k}} f^{(a)}_{A,\mathbf{k}'} f^{(a)\dagger}_{B,\mathbf{k}'+\mathbf{q}} f^{(a)}_{B,\mathbf{k}+\mathbf{q}} \\ & + 3J_z \sum_{\mathbf{k},\mathbf{k}',\mathbf{q},a} f^{(a)\dagger}_{A,\mathbf{k}} f^{(\bar{a})}_{A,\mathbf{k}'} f^{(\bar{a})\dagger}_{B,\mathbf{k}'+\mathbf{q}} f^{(a)}_{B,\mathbf{k}+\mathbf{q}} \\ & + 3J_z \sum_{\mathbf{k},\mathbf{k}',\mathbf{q},a} f^{(a)\dagger}_{A,\mathbf{k}} f^{(a)}_{A,\mathbf{k}'} f^{(\bar{a})\dagger}_{B,\mathbf{k}'+\mathbf{q}} f^{(\bar{a})}_{B,\mathbf{k}+\mathbf{q}} \\ & + \sum_{\mathbf{k},a} \left(n^{(a)}_{A,\mathbf{k}} + n^{(a)}_{B,\mathbf{k}}\right) + \text{const}, \end{aligned} \tag{8}$$

where a and $\bar{a}$ are the valley indices. This interaction consists of intervalley and intravalley interactions between the CS fermions.

To facilitate mean-field studies, we further resort to the band basis rather than the sublattice basis in the following calculations. The transformation is achieved via the unitary transformation $f^{(a)}_{\mathbf{k}} = U^{(a)}_{\mathbf{k}} \psi^{(a)}_{\mathbf{k}}$, where $f^{(a)}_{\mathbf{k}} = [f^{(a)}_{A,\mathbf{k}}, f^{(a)}_{B,\mathbf{k}}]^{\rm T}$ and $\psi^{(a)}_{\mathbf{k}} = [c^{(a)}_{+,\mathbf{k}}, c^{(a)}_{-,\mathbf{k}}]^{\rm T}$ are the spinors defined at valley a in the sublattice and band bases, respectively, and

$$U^{(a)}_{\mathbf{k}} = \frac{1}{\sqrt{2}} \begin{pmatrix} e^{-ia\theta} & -e^{-ia\theta} \\ 1 & 1 \end{pmatrix}, \tag{9}$$

with θ being the polar angle of $\mathbf{k}$. In this basis, H_0 is in its diagonalized form. Accordingly, $H_{\rm Ising}$ is also transformed into the band basis, whose form is shown in Appendix. In the band basis, it is clear that $H_{\rm Ising}$ involves different terms, e.g., the intravalley and interband interactions as well as the intervalley interactions. These interactions affect the Dirac fermions, and if they are strong enough, they could generate different fermionic orders. Besides, the gauge interaction $H_{\rm XY}$ in Eq. (5) competes with $H_{\rm Ising}$, which could drive the system towards a QPT. All in all, the quantum XXZ model in Eq. (1) has been fermionized to a low-energy spinless Dirac fermion theory with multiple fermion-fermion interactions, i.e., $H = H_0 + H_{\rm XY} + H_{\rm Ising}$.

IV. EXCITONIC INSTABILITY INDUCED BY THE ISING TERM

For the pure XY model, the effect of $H_{\rm XY}$ has been studied in Refs. [32,33,36,37]. To obtain intuition on the ground state for $J_z/J_x \gg 1$, we first analyze the possible effects on the Dirac fermions from $H_{\rm Ising}$ (which is the dominating interaction for $J_z/J_x \gg 1$) in this section.

$H_{\rm Ising}$ involves the interband interactions. It is known that the strong interband interaction between Dirac fermions can induce excitonic instabilities [38,39], thus we decouple $H_{\rm Ising}$ by introducing the mean-field orders in the particle-hole channel. We first consider the intravalley terms in $H_{\rm Ising}$, decoupling which requires the following intravalley mean-field orders as

$$\chi^{(a)}_{n,s} = \frac{3J_z}{2} \sum_{\mathbf{k}} \left\langle c^{(a)\dagger}_{n,\mathbf{k}} c^{(a)}_{\bar{n},\mathbf{k}} \right\rangle, \tag{10}$$

$$\lambda^{(a)}_{n,s} = \frac{3J_z}{2} \sum_{\mathbf{k}} \left\langle c^{(a)\dagger}_{n,\mathbf{k}} c^{(a)}_{n,\mathbf{k}} \right\rangle, \tag{11}$$

$$\boldsymbol{\chi}^{(a)}_{n,p} = \frac{3J_z}{2} \sum_{\mathbf{k}} \hat{\mathbf{k}} \left\langle c^{(a)\dagger}_{n,\mathbf{k}} c^{(a)}_{\bar{n},\mathbf{k}} \right\rangle, \tag{12}$$

where $\chi^{(a)}_{n,s}$ and $\boldsymbol{\chi}^{(a)}_{n,p}$ are the s-wave and the p-wave excitonic orders, respectively. Both the s- and p-wave pairings are allowed by symmetries and are considered here since the interaction terms with both s- and p-wave symmetry take place, as is shown in Appendix. From the above definitions, it is understood that $\chi^{(a)*}_{n,s} = \chi^{(a)}_{\bar{n},s}$ and $\boldsymbol{\chi}^{(a)*}_{n,p} = \boldsymbol{\chi}^{(a)}_{\bar{n},p}$.

With the introduced mean-field orders, the intravalley mean-field Hamiltonian can be obtained from $H_0 + H_{\rm Ising}$. Since in this mean-field channel the two valleys are effectively decoupled, we can simply consider each valley separately and make the valley notation a implicit. In the band basis $\psi_{\mathbf{k}} = (c_{+,\mathbf{k}} \quad c_{-,\mathbf{k}})^{\rm T}$, one obtains (see Appendix)

$$\begin{aligned} & H^{\rm intra}_{\rm MF} \\ & = \sum_{\mathbf{k}} \psi^{\dagger}_{\mathbf{k}} \begin{pmatrix} v_F k + \lambda_{-,s} & -\chi_s - \frac{1}{\sqrt{2}} \chi_p e^{-i\theta_k} \\ -\chi_s - \frac{1}{\sqrt{2}} \chi_p e^{i\theta_k} & -v_F k + \lambda_{+,s} \end{pmatrix} \psi_{\mathbf{k}} \\ & \quad + \frac{2}{3J_z} \chi_s^2 - \frac{2}{3J_z} \lambda_{+,s} \lambda_{-,s} + \frac{2}{3J_z} \chi_p^2, \end{aligned} \tag{13}$$

where we have used $\chi_s = \chi_{+,s} = \chi_{-,s}$ and χ_p is the amplitude of the order parameter $\boldsymbol{\chi}_{-,p} = \boldsymbol{\chi}^*_{+,p}$. The mean-field ground-state energy can be obtained from Eq. (13) as

$$\begin{aligned} E_G = {} & -\sum_{\mathbf{k}} \left\{ \lambda_1 + \left[\frac{1}{2} \chi_p^2 + \sqrt{2} \chi_p \chi_s \cos\theta \right. \right. \\ & \left. \left. + \chi_s^2 + (\lambda_2 + v_F k)^2 \right] \right\} \\ & + \frac{2}{3J_z} \chi_s^2 - \frac{2}{3J_z} (\lambda_1^2 - \lambda_2^2) + \frac{2}{3J_z} \chi_p^2, \end{aligned} \tag{14}$$

where we have introduced $\lambda_1 = \frac{1}{2}(\lambda_{+,s} + \lambda_{-s})$, $\lambda_2 = \frac{1}{2}(\lambda_{+,s} - \lambda_{-s})$.

With further introducing $\lambda_2 = \lambda_2' v_F \Lambda$, $\chi_p = \chi_p' v_F \Lambda$, $\chi_s = \chi_s' v_F \Lambda$, $J_z = J' v_F \Lambda$, $k = k' \Lambda$, and minimizing the mean-field ground-state energy, we arrive at the self-consistent equations for the order parameters in the continuum limit as

$$\begin{aligned} \lambda_2' &= \frac{3J'}{32\pi^2} \int k' dk' \int_0^{2\pi} d\theta \frac{\lambda_2' + k'}{\sqrt{A'}}, \\ \chi_p' &= \frac{3J'}{32\pi^2} \int k' dk' \int_0^{2\pi} d\theta \frac{\chi_p' + \sqrt{2}\chi_s' \cos\theta}{\sqrt{A'}}, \\ \chi_s' &= \frac{3J'}{32\pi^2} \int k' dk' \int_0^{2\pi} d\theta \frac{2\chi_s' + \sqrt{2}\chi_p' \cos\theta}{\sqrt{A'}}, \end{aligned} \tag{15}$$

where $A' = \chi_p'^2/2 + \sqrt{2}\chi_p' \chi_s' \cos\theta + \chi_s'^2 + (\lambda_2' + k')^2$.

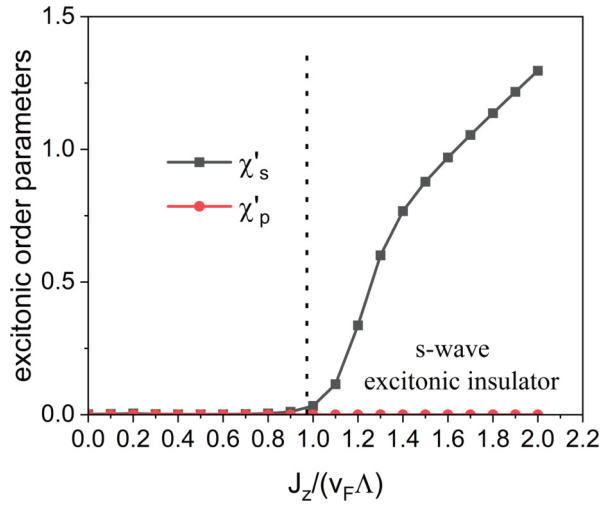

FIG. 3. Competition of the s- and p-wave excitonic orders in each valley. For large J_z, the s-wave excitonic order dominates, while the p-wave excitonic order is suppressed.

We self-consistently solve the equations in Eq. (15), and the results are shown in Fig. 3. λ_2' only exhibits a trivial solution and is hence not shown. Besides, as shown in Fig. 3, we find that no excitonic order can develop for $J_z/v_F\Lambda \lesssim 1$. This is because of the vanishing of the density of states at the Dirac nodes, making the interaction H_{Ising} irrelevant in the perturbative sense. For $J_z/v_F\Lambda \gtrsim 1$, the s-wave excitonic order is found to dominate over the p-wave excitonic order and nontrivial solution is developed only in the s-wave channel, suggesting that a CS s-wave exciton insulator state will be favored by the large interaction H_{Ising}.

We have considered above the intravalley interaction channel. We now take into account the intervalley terms and introduce an additional order parameter (see Appendix)

$$\bar{\boldsymbol{\chi}}_{n,p}^{(a)} = \frac{3J_z}{2}\sum_{\mathbf{k}} \hat{\mathbf{k}} \left\langle c_{n,\mathbf{k}}^{(a)\dagger} c_{\bar{n},\mathbf{k}}^{(\bar{a})} \right\rangle \tag{16}$$

which describes an intervalley excitonic state. Interestingly, because of the symmetry of the intervalley interactions, the p-wave pairing must be considered, which arises from the decomposition of the intervalley terms in H_{Ising}.

With the intervalley terms taking into account, the effective mean-field Hamiltonian is now given by

$$H_{\text{MF}} = \sum_{\mathbf{k}} \Psi_{\mathbf{k}}^{\dagger}\mathcal{H}\Psi_{\mathbf{k}} + \frac{2}{3J_z}(\chi_s^{(+)} + \chi_s^{(-)})^2 + \frac{4}{3J_z}\bar{\boldsymbol{\chi}}_p^{(+)} \cdot \bar{\boldsymbol{\chi}}_p^{(-)}, \tag{17}$$

where $\Psi_{\mathbf{k}} = (c_{+,\mathbf{k}}^{(+)} \quad c_{-,\mathbf{k}}^{(+)} \quad c_{+,\mathbf{k}}^{(-)} \quad c_{-,\mathbf{k}}^{(-)})^{\text{T}}$, and

$$\mathcal{H} = \begin{pmatrix} v_F k & -\sum_a \chi_s^{(a)} & 0 & -\bar{\boldsymbol{\chi}}_p^{(+)} \cdot \hat{\mathbf{k}} \\ -\sum_a \chi_s^{(a)} & -v_F k & -\bar{\boldsymbol{\chi}}_p^{(+)} \cdot \hat{\mathbf{k}} & 0 \\ 0 & -\bar{\boldsymbol{\chi}}_p^{(-)} \cdot \hat{\mathbf{k}} & -v_F k & \sum_a \chi_s^{(a)} \\ -\bar{\boldsymbol{\chi}}_p^{(-)} \cdot \hat{\mathbf{k}} & 0 & \sum_a \chi_s^{(a)} & v_F k \end{pmatrix}, \tag{18}$$

where we have used $\chi_{\pm,s}^{(a)} = \chi_s^{(a)}$ and $\bar{\boldsymbol{\chi}}_{\pm,p}^{(a)} = \bar{\boldsymbol{\chi}}_p^{(a)}$. The entries $\pm\sum_a \chi_s^{(a)}$ in the above matrix involve the sum of the s-wave excitonic orders at both valleys. The two terms in the sum come from the contributions of the intervalley and intravalley interaction terms in H_{Ising}, respectively (see Appendix). To simplify notation, we introduce $\bar{\chi}_s = \chi_s^{(+)} + \chi_s^{(-)}$, which in general describes the intravalley excitonic order.

Again by minimizing the ground-state energy, we can obtain the self-consistent equations with respect to $\bar{\chi}_s$ and $\bar{\chi}_p$, with the latter being the amplitude of the intervalley excitonic order $\bar{\boldsymbol{\chi}}_p$, namely,

$$\begin{aligned} \bar{\chi}_s &= \frac{3J_z}{4}\sum_{\mathbf{k}}\left(\frac{\bar{\chi}_s}{\bar{\chi}_s^2 + (\bar{\chi}_p + k)^2} + \frac{\bar{\chi}_s}{\bar{\chi}_s^2 + (\bar{\chi}_p - k)^2}\right), \\ \bar{\chi}_p &= -\frac{3J_z}{8}\sum_{\mathbf{k}}\left(\frac{\bar{\chi}_p + k}{\bar{\chi}_s^2 + (\bar{\chi}_p + k)^2} + \frac{\bar{\chi}_p - k}{\bar{\chi}_s^2 + (\bar{\chi}_p - k)^2}\right). \end{aligned} \tag{19}$$

Solving the above self-consistency equations, we can readily prove that the intervalley p-wave excitonic order is also dominated by the intravalley s-wave order for large J_z, similar to results shown in Fig. 3.

So far, we have found that by considering $H_0 + H_{\text{Ising}}$, the most favorable instability of the Dirac CS fermions is the intravalley s-wave excitonic pairing, giving rise to an excitonic insulator state with a s-wave gap. Since the pairing is mainly dominated by intravalley processes, the two valleys are essentially separable from each other because the $\bar{\chi}_p$ terms vanish in Eq. (18). The mean-field Hamiltonian for such a state is therefore derived as

$$\mathcal{H}_{\text{eff}} = v_F k_x \tau_z \sigma_x + v_F k_y \tau_0 \sigma_y + \bar{\chi}_s \tau_0 \sigma_z, \tag{20}$$

where we have transformed the mean-field Hamiltonian from the band basis back to the sublattice basis. τ_α and σ_β are the Pauli matrices acting on the valley and sublattice spaces, respectively.

It is important to discuss the topology and symmetry of Eq. (20). First, the CS exciton insulator has two gapped Dirac nodes in low energy. Each of the gapped Dirac nodes carries an effective $\pm\frac{1}{2}$ Chern number due to the parity anomaly in 2D, where the sign in front is determined by the sign of the Dirac mass. Besides, it is readily seen that $\mathcal{H}_{\text{eff}}$ respects the time-reversal symmetry (TRS). Thus, the Chern number from the two gapped Dirac fermions cancels each other, leading to $C = \frac{1}{2} - \frac{1}{2} = 0$, namely, a topologically trivial CS excitonic insulator. This is expected since the original spin system remains topologically trivial as we enlarge the Ising interaction H_{Ising}.

Here, we mention in passing that Ref. [35] studies the J_1-J_2 XY model on the honeycomb lattice with a flux perturbation. A similar excitonic insulator phase is found in the CS fermion representation but with nonzero Chern number $C = 1$. However, our case here is different from that considered in Ref. [35] in two senses. First, the physical origins of the excitonic pairing are different. The excitonic state in our case is induced by the Ising interaction rather than by the next-nearest-neighbor XY term in Ref. [35]. Second, our case is further complicated by more intervalley interaction terms, which can be decoupled into both an intervalley p-wave and an intravalley s-wave excitonic order. Interestingly, the intravalley interaction terms also favor the s-wave excitonic order, finally resulting in the term $\bar{\chi}_s = \sum_a \chi_s^{(a)}$ in Eq. (18).

This particular structure in terms of the order parameter $\bar{\chi}_s$ is a key feature of the Ising interaction H_{Ising}, which is in stark contrast with that of the J_1-J_2 XY model. This structure ensures that the CS excitonic insulator found in our case enjoys Dirac masses of the same sign at the two valleys, which in turn guarantees $C = 0$. Therefore, $C = 0$ is a direct consequence of H_{Ising}, which essentially reflects the fact that no topological nontrivial states can arise in the nonfrustrated XXZ model on bipartite lattices. This also confirms the crucial role of frustration in generating topological states in the Chern-Simons mean-field theories.

V. PHASE TRANSITIONS CAUSED BY VARYING THE STRENGTH OF THE ISING TERM

So far, we have investigated the effects of the Ising term, i.e., $H_0 + H_{\text{Ising}}$, in the language of CS fermions, and we have found that it induces the s-wave excitonic order of the Dirac CS fermions. This phase should only apply to the region where $J_z/J_x \gg 1$. To examine whether there are any QPTs in the intermediate J_z/J_x regime, one has to fully consider the total Hamiltonian $H = H_0 + H_{\text{Ising}} + H_{\text{XY}}$.

$H_0 + H_{\text{XY}}$ has been studied by Refs. [32,33,36,37], where it is shown that the CS superconductor state is stabilized, which serves as a description of the planar Néel AFM state in the CS fermion representation. From these previous results, we can readily derive the full mean-field Hamiltonian describing the XXZ quantum magnets in the full parameter range. We resort to the sublattice⊗Nambu basis $\mathbf{\Psi_k} = (f^{(+)}_{\mathbf{k},A} \quad f^{(+)}_{\mathbf{k},B} \quad f^{(-)\dagger}_{-\mathbf{k},A} \quad f^{(-)\dagger}_{\mathbf{k},B})^{\mathrm{T}}$, in which we can deduce the following Bogoliubov–de Gennes Hamiltonian:

$$\mathcal{H}_{\text{BdG}} = \begin{pmatrix} \bar{\chi}_s & v_F k e^{-i\theta} & \Delta_3 & \Delta_{0k} e^{-i\theta} \\ v_F k e^{i\theta} & -\bar{\chi}_s & -\Delta_{0k} e^{i\theta} & \Delta_3 \\ \Delta_3 & -\Delta_{0k} e^{-i\theta} & -\bar{\chi}_s & -v_F k e^{-i\theta} \\ \Delta_{0k} e^{i\theta} & \Delta_3 & -v_F k e^{i\theta} & \bar{\chi}_s \end{pmatrix}, \tag{21}$$

that not only involves the CS superconductor mean-field state but also the CS excitonic order derived above. The lowest two eigenvalues of $\mathcal{H}_{\text{BdG}}$ are readily obtained as

$$E_{\pm,k} = -\sqrt{\left[\sqrt{\bar{\chi}_s^2 + (v_F k)^2} \pm \Delta_{0k}\right]^2 + \Delta_3^2}. \tag{22}$$

Three order parameters emerge in the above effective theory, i.e., Δ_{0k}, Δ_3, and $\bar{\chi}_s$, where Δ_{0k} (Δ_3) is the off-diagonal (diagonal) component of the superconducting gap in the sublattice, and $\bar{\chi}_s$ is the intravalley s-wave excitonic order, which has been shown to be the most relevant instability favored by H_{Ising}. These order parameters are governed by the coupled self-consistent equations in the continuum limit as

$$\begin{aligned} \bar{\chi}_s &= -\frac{3J_z}{2} \sum_{k,a=\pm} \frac{\bar{\chi}_s \left[1 + a\Delta_{0k}/\sqrt{\bar{\chi}_s^2 + (v_F k)^2}\right]}{E_{a,k}}, \\ \Delta_3 &= -\frac{e}{2} \sum_{k,a=\pm} \frac{\Delta_{0k} + a\sqrt{\bar{\chi}_s^2 + (v_F k)^2}}{E_{a,k}}, \\ \Delta_{0k} &= \frac{1}{4} e v_F k \frac{\Delta_3}{\sqrt{\bar{\chi}_s^2 + \Delta_3^2}}. \end{aligned} \tag{23}$$

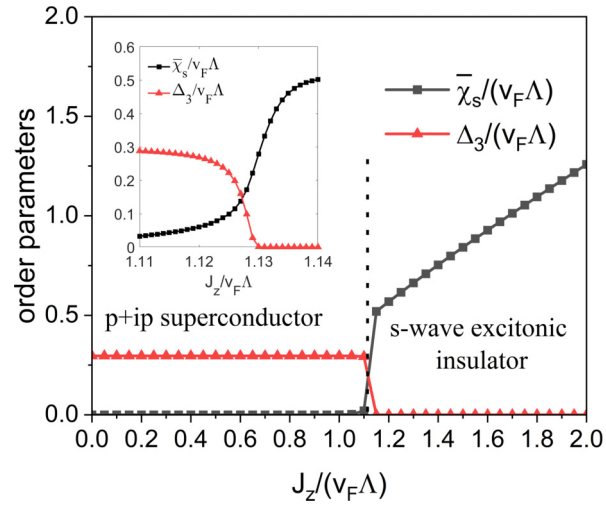

FIG. 4. A phase transition takes place as J_z is increased. When J_z is relatively small, the $p + ip$ CS superconductor state coexists with the excitonic order, with the former dominating over the latter. When J_z is large enough, the excitonic insulator state dominates, and the CS superconductor state is totally suppressed. The inset shows the order parameters in the zoom-in region near the transition point.

We self-consistently solve the above equations with varying J_z and plotted the order parameters against J_z in Fig. 4. Because Δ_{0k} is completely determined by Δ_3 and $\bar{\chi}_s$, and it vanishes as $k \to 0$, only Δ_3 and $\bar{\chi}_s$ need to be plotted. As shown in Fig. 4, when J_z is small, the CS superconductor state dominates. Interestingly, for large $J_z/v_F\Lambda$, the CS superconductor state is suppressed by the excitonic state, and the CS excitonic insulator state becomes stable after crossing the transition point. Since it is known that CS superconductors can describe the planar Néel state in the spin language, this indicates that the planar spin ordering should be destabilized for large H_{Ising}, in accordance with the DMRG calculation in Fig. 1.

To understand the physical nature of the transition in Fig. 4, we notice that the s-wave excitonic insulator has a clear physical counterpart in the spin picture. This CS exciton insulator is described by Eq. (20), which enjoys a mass term $\bar{\chi}_s \tau_0 \sigma_z$. The Pauli matrix σ_z introduces opposite onsite potentials for the CS fermions on the A and B sublattices, namely, a charge density wave order of the CS fermions. With $\bar{\chi}_s = 0$, the fermion system is half-filled with averaged density $\langle n \rangle = \frac{1}{2}$. The nonzero $\bar{\chi}_s$ therefore brings about sublattice-dependent fluctuations of the charge density around $\langle n \rangle = \frac{1}{2}$. Noting that the fermion density is related to S^z via $S^z_i = n_i - \frac{1}{2}$, the charge order is directly translated into an out-of-plane Néel Ising ordering in the spin picture, as shown by the inset of Fig. 1.

Given the above observations, we conclude that the CS fermion mean-field theory also reveals a QPT from the in-plane to the out-of-plane Néel AFM order, in agreement with the numerical results. Interestingly, the fermionic theory endows such a QPT with a fermionic mean-field interpretation, i.e., from a CS superconductor state to a CS excitonic insulator state.

VI. GENERALIZATIONS TO OTHER LATTICES

So far, we have demonstrated how the CS mean-field theory is applied to the XXZ model on the honeycomb lattice.

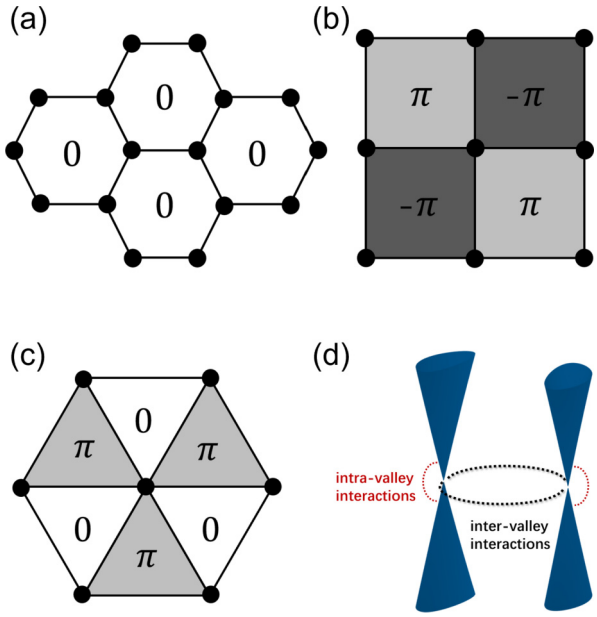

FIG. 5. The flux states on (a) honeycomb, (b) square, and (c) triangular lattices. As shown in (d), at low energy, the Dirac nodes take place for all three lattices, which is further subjected to gauge-mediated interactions after restoring the gauge fluctuations.

However, we emphasize that the applicability of our method is not only limited to the honeycomb lattice. In this section, we will discuss generalizations of our method to other lattices, taking the square and triangular lattices as examples.

As demonstrated above, CS fermionization maps spin-$\frac{1}{2}$ operators to spinless fermions coupled to emergent CS gauge field. Here, a good starting point is to ignore the gauge fluctuations and regard the gauge field as static fluxes coupled to the fermions. Then, by minimizing the energy of the fermions, one can arrive at flux states on two-dimensional (2D) lattices. Taking the honeycomb, square, and triangular lattices as examples, the most energetically favorable flux states are plotted in Figs. 5(a)–5(c), respectively. On the honeycomb lattice, the flux in each plaquette is zero; on the square lattice, staggered π flux are known to be most favorable [40], while on the triangular lattice, the staggered 0-π flux state has been found in Ref. [29] to be most favorable. For all the above flux states, low-energy Dirac fermions take place, as indicated by Fig. 5(d). Thus, it is clear that the low-energy Dirac fermions are not merely associated to the honeycomb lattice geometry. Instead, they essentially originate from the CS fluxes, which modify the kinetic energies of the fermions. Here, we note that the triangular lattice case is a bit more complicated, as the 0-π flux state in Fig. 5(c) generates two Dirac nodes in the first Brillouin zone, which further enjoy threefold degeneracy. Although this brings about some complications, the procedures remain the same as those for the honeycomb and square lattice cases.

Then, we go beyond the above mean-field treatment of fluxes and further consider gauge fluctuations. This leads to gauge-mediated interactions shown in Eq. (5), as well as the Ising interactions shown in Eq. (7). The mean-field approach we have demonstrated for the honeycomb lattice then applies naturally to the square and triangular lattices. Taking the square lattice as an example, the flux states in Fig. 5(b) are reduced to the following low-energy description:

$$H_0 = v_F \sum_{\mathbf{k}} (f_{\mathbf{k}}^{(+)\dagger} \mathbf{k}\cdot\boldsymbol{\sigma} f_{\mathbf{k}}^{(+)} + f_{\mathbf{k}}^{(-)\dagger} \mathbf{k}\cdot\boldsymbol{\sigma}^T f_{\mathbf{k}}^{(-)}), \tag{24}$$

where $f_{\mathbf{k}}^{(\pm)}$ denotes the fermionic annihilation operator in the $\pm$ valley, and $v_F = 2Ja$ with a being the lattice spacing of the square lattice. This is in the same form as Eq. (4) for the honeycomb case.

The CS gauge-field-mediated interaction term is also found to enjoy a similar form as Eq. (5), which also has the vertex with $p + ip$ symmetry, i.e.,

$$V_{\mathbf{q}}^{\alpha\alpha'\beta'\beta} = -\pi i e v_F \epsilon^{ij} \left(\sigma^i_{\alpha\beta}\delta_{\alpha'\beta'} - \delta_{\alpha\beta}\sigma^i_{\alpha'\beta'}\right) A^j_{\mathbf{q}}. \tag{25}$$

Furthermore, the Ising term is transformed accordingly into

$$H_{\text{Ising}} = 2J_z \sum_{\mathbf{r}} (f^\dagger_{A,\mathbf{r}} f_{A,\mathbf{r}} - 1/2)(f^\dagger_{B,\mathbf{r}} f_{B,\mathbf{r}} - 1/2). \tag{26}$$

Comparing the fermionized XXZ models for the square and honeycomb lattices, we find that they only exhibit slight differences in coefficients, such as those in H_{Ising} and the effective Fermi velocity v_F. Therefore, all the derivations and the resulting mean-field theories remain the same. The analysis above shows that the presented theory is generalizable to other lattices, and thus could provide a guidance to QPTs in quantum magnets, at least for a certain class of spin models.

Lastly, we mention that the CS fermion mean-field approach is also applicable to cases with further neighbor exchange interactions. For example, the CS fermionzation has been carried out for J_1-J_2 XY model on the honeycomb lattice [35]. Despite the presence of the H_{XY} interaction in Eq. (5), another gauge-mediated interaction takes place, which was found to generate a topological phase transition towards possible chiral spin liquids under proper perturbations.

VII. NATURE OF THE TRANSITION

In the above section, we have applied the Chern-Simons mean-field theory of XXZ models to several different lattices. The fermionic mean-field orders were proposed for both the planar and out-of-plane Néel AFM orders on the two sides of the transition. In the following, we discuss how the fermionized theory enhances our understanding of the nature of the QPT, with additional support from numerical simulations.

A. CS fermion-indicated O(3) nonlinear σ model

We take the honeycomb lattice as an example. As the first step, we solve the mean-field equations, i.e., Eq. (23), in the vicinity of the critical point. As shown by the inset to Fig. 4, we observe that the CS superconductor order parameter is gradually replaced by the excitonic insulator order parameter. The slow evolution of the order parameters near the transition point $J_z/J_x \sim 1$ indicates that the symmetries of effective field theories on the two sides can be smoothly "rotated" into each other.

Then, we revisit the CS superconductor state for $J_z/J_x < 1$, from the perspective of effective field theories. By turning off the excitonic order χ in Eq. (22) in the long-wave regime,

the mean-field ground state is described by Bogoliubov quasiparticles with the energy gap Δ_3. Following the standard way of deriving the Ginzberg-Landau theory of superconductors, the Bogoliubov fields can be integrated out, leading to the effective free energy as

$$\mathcal{F} = \int d^2x \frac{1}{2}|\nabla\Psi(\mathbf{x})|^2 + \frac{m}{2}|\Psi(\mathbf{x})|^2 + \frac{g}{4}|\Psi(\mathbf{x})|^4, \quad (27)$$

where $\Psi(\mathbf{x})$ is the complex order parameter field describing the CS superconductor and m and g are Ginzberg parameters that are determined from those of the original CS fermions. Inserting $\Psi = \Delta_3 e^{i\theta}$, where Δ_3 and θ are the modulus and phase of Ψ, respectively, $|\nabla\Psi|^2$ can be approximately written as $(\partial_\mu \mathbf{n}_{sc})^2$, where $\mathbf{n}_{sc} = (n_1, n_2)$, with $n_1 = \Delta_3$ and $n_2 = \Delta_3\theta$, namely, $n_1 = \mathrm{Re}[\Psi]$ and $n_2 = \mathrm{Im}[\Psi]$ for $\theta \sim 0$. We note that in the CS superconductor state, the order parameter $\Psi(\mathbf{x}) \sim \Delta_3$ is formed with real gauge. Thus, $(\partial_\mu \mathbf{n}_{sc})^2$ actually describes the fluctuations around the mean-field order parameter $\Psi(\mathbf{x}) \sim \Delta_3$, leading to the collective modes which have been studied in Refs. [33,36]. Thus, Eq. (27) is cast into

$$\mathcal{F} = \int d^2x \left(\frac{1}{2}\nabla \mathbf{n}_{sc}\right)^2 + \frac{m}{2}n_{sc}^2 + \frac{g}{4}n_{sc}^4, \quad (28)$$

where $n_{sc} = n_\mu n_\mu$, $\mu = 1, 2$, and repeated indices are summed. Equation (28) describes a ϕ^4-type theory with O(2) symmetry. Since the superconductor state is developed, the initially degenerate fluctuations decompose into a massive Higgs mode, i.e., the radial fluctuations of n_{sc}, as well as a Glodstone mode in terms of the fluctuations of the unit vector $\hat{\mathbf{n}}_{sc} \equiv \mathbf{n}_{sc}/n_{sc}$. This symmetry breaking is achieved by taking the large negative m in Eq. (28), which leads to the following effective theory:

$$\mathcal{F}_{\mathrm{eff}} = \beta\mathcal{H}_{\mathrm{eff}} = \int d^2x \frac{K}{2}(\nabla\hat{\mathbf{n}}_{sc})^2 + \mathrm{const}, \quad (29)$$

where $\beta = 1/T$, and $K = n_{sc}^2$ is the effective coupling constant. Clearly, this is a nonlinear sigma model (NLσM) with O(2) symmetry.

The above shows that the effective field theory describing the CS superconductor phase can be described by a O(2) NLσM, where the O(2) vector is defined by the CS superconductor order parameter $\mathbf{n}_{sc} = (n_1, n_2) = (\mathrm{Re}[\Psi], \mathrm{Im}[\Psi])$. We then recall that, on the other side of the transition, an excitonic insulator is obtained in the CS fermionic mean-field theory, which only exhibits a single scalar order parameter χ. Since $\pm\chi$ describe degenerate excitonic states in accord with $\pm\langle S^z\rangle$ Ising configuration, the effective theory of the excitonic insulator in terms of χ should only enjoy O(1) symmetry, whose fundamental representations are real numbers ± 1. Besides, we have previously observed that the symmetries of the CS superconductor and the excitonic insulator can be smoothly "rotated" into each other near $J_z/J_x \sim 1$, thus it is natural to construct a O(3) NLσM, which describes the QPT in the fermionic language.

We thus introduce the vector $\mathbf{n} = (n_1, n_2, n_3) = (\mathrm{Re}[\Psi], \mathrm{Im}[\Psi], \chi)$, which consists of both the order parameters of the CS superconductor and the excitonic insulator. Accordingly, the "superspin" [41,42] is defined as $\hat{\mathbf{n}} = \mathbf{n}/n$, where $n = \sqrt{n_\mu n_\mu}$ with $\mu = 1, 2, 3$. Then, the O(3) NLσM emerges naturally in the CS fermion mean-field theory as

$$\beta\mathcal{H}_{\mathrm{eff}}^{\mathrm{tot}} = \frac{K}{2}\int d^2x(\nabla\hat{\mathbf{n}})^2 + \lambda\int d^2x\left[n_{sc}^2 - n_3^2\right]/n^2, \quad (30)$$

where the λ term is introduced as the tuning parameter that drives the phase transition. For $\lambda = 0$, Eq. (30) describes the transition point, which enjoys the O(3) symmetry corresponding to the original Heisenberg Hamiltonian at $J_z/J_x = 1$. One notes that the time variation of superspin is negligible since the model enters the renormalized classical regime for the ordered states [43]. For $\lambda > 0$, n_3^2, thus the CS excitonic insulator order is more favorable, which breaks the O(3) symmetry down to O(1). For $\lambda < 0$, n_{sc}^2, thus the CS superconductor is more favorable and the O(3) symmetry is broken down to O(2).

Equation (30) sheds light on the nature of the transition at $J_z/J_x = 1$. We perform a perturbative renormalization group (RG) analysis of the O(N) model while turning off λ, which generates the RG flow $\frac{dK}{dl} = (2-N)/2\pi$. For the Heisenberg point where $\lambda = 0$, the model has O(3) symmetry with $N = 3$. In this case, the stiffness K is irrelevant. The system thus stays at the weak coupling (or high-temperature) fixed point and remains disordered. In comparison, for $\lambda > 0$, the symmetry is effectively reduced to $O(1)$, thus K becomes relevant, flowing to the ordered state corresponding the excitonic insulator with nonzero χ. For $\lambda < 0$, the remaining symmetry is O(2). With $N = 2$, K becomes marginal. This reflects the Kosterlitz-Thouless nature of the ordering of the 2D XY model. Interestingly, the vortex and antivortex in the original spin picture are equivalently interpreted to be the vortex excitations of CS superconductors.

As shown above, starting from the CS fermion mean-field theory, one can systematically solve the mean-field orders, which further serve as the building blocks to construct the field theory describing the QPTs. For the XXZ model, the theory indicates a continuous transition at $J_z/J_x = 1$ where the O(3) symmetry is restored. In the following, we present DMRG calculations to further confirm the above analytic conclusion.

B. Numerical study of the nature of the QPT

We now numerically study the phase transition at $J_z/J_x = 1$ using DMRG. The nature of the transition is determined by how the ground-state wave function is changed across the critical point. This can be numerically probed by calculating the fidelity [44–62]. In general, considering a Hamiltonian consisting of a tuning parameter λ, the quantum fidelity is defined as the overlap of ground states at neighboring parameters, i.e.,

$$F(\lambda, \delta\lambda) = |\langle\Psi_0(\lambda)|\Psi_0(\lambda + \delta\lambda)\rangle|. \quad (31)$$

$F(\lambda, \delta\lambda)$ displays singular behaviors in the vicinity of the critical point. Due to the discrepancy of ground states on different sides of transition point, the fidelity usually exhibits a steep drop around the critical point. In the limit of $\delta\lambda \to 0$, the fidelity can be further expanded as

$$F(\lambda, \delta\lambda \to 0) \simeq 1 - \tfrac{1}{2}\chi_F(\lambda)\delta\lambda^2, \quad (32)$$

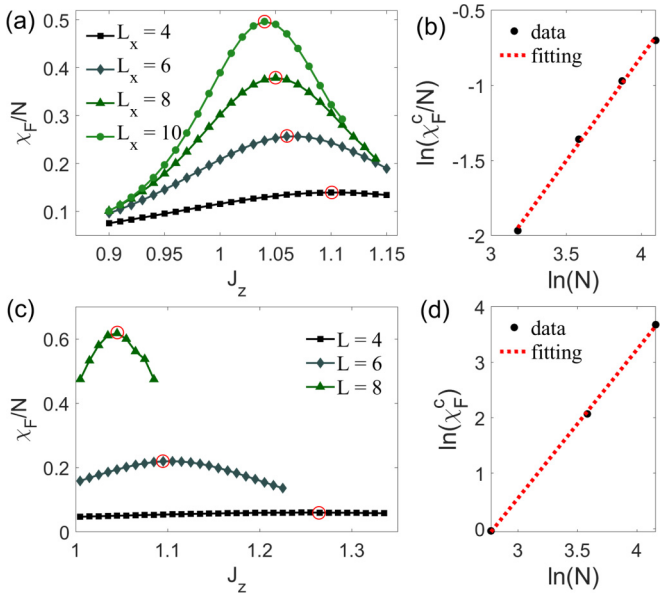

FIG. 6. (a) Calculated fidelity susceptibility per site as a function of J_z for nearest-neighbor spin-$\frac{1}{2}$ XXZ model on honeycomb lattice. Results for different system sizes are shown. The red circles highlight the maxima of χ_F/N, which gradually approach the exact critical point $J_z/J_x = 1$ with increasing system sizes. (b) The scaling of fidelity susceptibility at the critical point [determined by the maxima of χ_F/N in (a)] with respect to the number of lattice sites N. (c), (d) The fidelity susceptibility and its scaling obtained for the nearest-neighbor spin-$\frac{1}{2}$ XXZ model on square lattice, respectively. The results in (d) lead to the critical exponent $1/\nu = \ln \chi_F^c / \ln N = 2.675$.

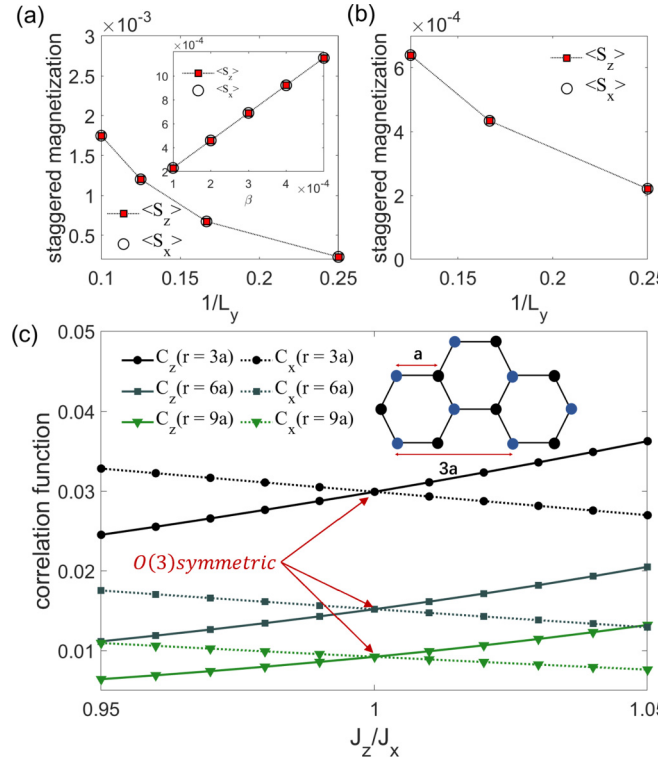

FIG. 7. (a), (b) Show $\langle S_{x,z} \rangle$ for different L_y with $L_x = 4$, for the honeycomb and the square models, respectively. The same pinning field $\beta = 10^{-4}$ is introduced along both the x and the z directions. The inset to (a) shows the changes of $\langle S_{x,z} \rangle$ with increasing pinning field β. (c) The DMRG results of the correlation function $C_{x,z}(\mathbf{r}) = \langle S_{x,z}(0) S_{x,z}(\mathbf{r}) \rangle$ for the honeycomb model, where $\mathbf{r}$ is taken as 3,6,9 lattice spacings along the L_x direction as indicated by the inset to (c). The system size is $L_y = 4$, $L_x = 8$.

where the coefficient of the $\delta\lambda^2$-order term, i.e., $\chi_F(\lambda)$, is termed as the fidelity susceptibility (FS). $\chi_F(\lambda)$ describes the rate of change of the fidelity under infinitesimal variations of λ. Clearly, the drop in the fidelity near the critical point is manifested by the divergent behavior of $\chi_F(\lambda)$. From the peaks of FS obtained in numerical simulations, one can determine the location of the transition point. We mention in passing that, although the transition point obtained in this way usually exhibits some deviations from its exact value due to finite-size effects, such deviations decrease gradually and we approach the exact critical point as the system size increases.

Importantly, scaling theory in terms of FS has been studied in [56–59]. For all second-order QPTs, the FS per site near the critical point obeys the scaling law

$$\chi_F/N \sim L^{2/\nu - d}, \tag{33}$$

where N is the number of lattice sites, L is the system size, d is the spatial dimension of the system, and ν is the critical exponent of the correlation length. Thus, for $N \sim L^2$, a linear relationship between $\ln \chi_F$ and $\ln N$ is expected to take place near the critical point. In particular, for $N \sim L^2$ and $d = 2$, $\chi_F \sim L^{2/\nu}$, thus $\ln \chi_F \sim \frac{1}{\nu} \ln N$. The linear dependence can be used as a criterion for second-order QPTs, and this criterion has been used in different correlated systems [56–59].

We perform the DMRG calculations of the FSs for both the honeycomb and the square lattices with different system sizes. As shown by Figs. 6(a) and 6(c), χ_F/N exhibits significant peaks for both the honeycomb and the square lattices, which approaches $J_z/J_x = 1$ with increasing system sizes. Moreover, we observe the linear dependence between $\ln \chi_F$ and $\ln N$ for both lattices, as shown in Figs. 6(b) and 6(d). This clearly demonstrates that the phase transition at $J_z/J_x = 1$ between the planar Néel AFM and the out-of-plane AFM order to be a continuous QPT, in accordance with the field-theoretical result. Here, we also mention in passing that, from Fig. 6(d), the critical exponent is extracted to be $1/\nu = 2.675$ for the square lattice case. This is in accurate agreement with the quantum Monte Carlo simulations of the model [57], which obtains $1/\nu = 2.68(6)$.

Our CS fermion-indicated NLσM suggests a restored O(3) symmetry at $J_z/J_x = 1$. This can also be verified numerically. First, we note that the order parameters $\langle S_x \rangle$, $\langle S_z \rangle$ in Fig. 1 are obtained by applying a weak pinning field $\beta \sim 10^{-4}$ along the x direction, which favors the planar Néel order. This leads to the numerical artifact that the order $\langle S_x \rangle$ dominates at $J_z/J_x = 1$. Thus, we refine the calculations of the order parameters at $J_z/J_x = 1$, by applying equal pinning fields ($\beta \sim 10^{-4}$) along both the x and z directions. As shown by Figs. 7(a) and 7(b), for both the honeycomb and the square lattices with different system sizes, $\langle S_x \rangle$ and $\langle S_z \rangle$ are found to be exactly equal to each other at $J_z/J_x = 1$. Besides, their values are small and depend only on the pinning field. This is clear from the linear growth of $\langle S_{x,z} \rangle$ with β shown in the inset to Fig. 7(a).

Thus, the system has an equal preference in terms of $\langle S_x \rangle$ and $\langle S_z \rangle$ at the Heisenberg point, in agreement with the O(3) NLσM. Besides, we also calculate the correlation function $\langle S_{x,z}(0) S_{x,z}(\mathbf{r}) \rangle$ for different distances $|\mathbf{r}| = 3a, 6a, 9a$, where a is the lattice spacing. As shown by Fig. 7(c), we find that $\langle S_x(0) S_x(\mathbf{r}) \rangle = \langle S_z(0) S_z(\mathbf{r}) \rangle$ is exactly satisfied at $J_z/J_x = 1$. This also clearly demonstrates the O(3) symmetry at the critical point.

VIII. SUMMARY AND DISCUSSION

We have generalized the CS fermionization method to study the quantum XXZ model. Previously, this fermionization approach has only been used to explore the ideal XY models [32,33,36]. In comparison, the XXZ models differ from the XY models after fermionization, mainly because of the complications brought about by the additional Ising interaction. The Ising interaction generates an additional local fermion-fermion interaction, which in turn leads to multiple possible instability channels that are allowed by symmetries. Through careful analysis, we found that it is the intravalley s-wave excitonic channel that is most energetically favorable. Accordingly, an interesting phase transition from the CS superconductor state to the CS s-wave excitonic insulator state is discovered. We propose that this phase transition provides a fermionic interpretation of the QPT from the planar Néel AFM to the out-of-plane Néel order.

The CS fermion approach also suggests a systematic way to obtain field-theoretical understandings of the nature of the QPTs. Using the order parameters obtained in the CS fermion mean-field theory, we propose a NLσM in terms of the O(3) superspin that describes the QPT in the XXZ model. Numerical simulations are also performed, which clearly demonstrates the continuous nature of the QPT as well as the O(3) symmetry at the Heisenberg point. Lastly, the method proposed here is generalizable to different lattices. Although we show analytic and numerical results for the square and the honeycomb lattices as examples, we note that generalizations to other cases, such as the triangular lattice, are also possible. The latter has in fact been proved to display Dirac nodes in terms of CS fermions after CS fermionization [33], which already paves the way for further studies on the QPTs driven by other interactions.

Last, it should be further mentioned that the CS fermion approach is technically different from the parton approaches. The latter has been used to understand ordered state starting from a parent spin-liquid state [21,22]. In analogy, here we show that the Dirac CS fermions state as indicated by Fig. 5(d) can be used as a parent state to generate the magnetically ordered states. Despite the similarities between the two approaches, the CS representation does not require additional constraint conditions on local Hilbert space. Thus, it may yield more straightforward mean-field descriptions of ordered states, without the need of further Gutzwiller projections. Therefore, purely fermionic theories in faithful representation of the microscopic spin models become likely, which, as illustrated above, provide a systematic way to understand QPTs in quantum magnets.

In summary, our generalized CS fermionization method has produced results absent in previous CS mean-field theories. It provides different understandings of QPTs in quantum XXZ magnets from perspective of fermions. The generalization from the XY models to the XXZ models made here could have far-reaching consequences, as it is an indispensable step essential for the CS fermion mean-field theories to be applicable to realistic magnetic materials. Based on the results in this work, and with further neighbor interactions being taken into account, the CS fermion theory could enjoy many versatile applications and provide useful descriptions for frustrated quantum magnets that are of experimental relevance.

ACKNOWLEDGMENTS

R.W. is grateful to T. Sedrakyan and Q.-H. Wang for fruitful discussions. This work was supported by National Natural Science Foundation of China (Grant No. 11904225), the Innovation Program for Quantum Science and Technology (Grant No. 2021ZD0302800), and the National Key R&D Program of China (Grant No. 2017YFA0303200).

APPENDIX: TECHNICAL DETAILS IN THE DERIVATION OF THE EFFECTIVE HAMILTONIAN

In the main text, upon CS fermionization and the projection to the low-energy window around the two Dirac valleys, H_{Ising} can be expressed by CS fermions as Eq. (8). We then transform it to the band basis, and after appropriate rearrangements, we obtain four kinds of interactions:

$$
\begin{aligned}
V^{(1)} &= -\frac{3J_z}{4} \sum_{a,n,\mathbf{k},\mathbf{k}'} c^{(a)\dagger}_{n,\mathbf{k}} c^{(a)}_{\bar{n},\mathbf{k}} c^{(a)\dagger}_{\bar{n},\mathbf{k}'} c^{(a)}_{n,\mathbf{k}'} \\
&\quad + \frac{3J_z}{4} \sum_{a,n,\mathbf{k},\mathbf{k}'} c^{(a)\dagger}_{n,\mathbf{k}} c^{(a)}_{n,\mathbf{k}} c^{(a)\dagger}_{\bar{n},\mathbf{k}'} c^{(a)}_{\bar{n},\mathbf{k}'}, \\
V^{(2)} &= -\frac{3J_z}{4} \sum_{a,n,\mathbf{k},\mathbf{k}'} \mathbf{k}\cdot\mathbf{k}' c^{(a)\dagger}_{n,\mathbf{k}} c^{(a)}_{\bar{n},\mathbf{k}} c^{(a)\dagger}_{\bar{n},\mathbf{k}'} c^{(a)}_{n,\mathbf{k}'} \\
&\quad + \frac{3J_z}{4} \sum_{a,n,\mathbf{k},\mathbf{k}'} \mathbf{k}\cdot\mathbf{k}' c^{(a)\dagger}_{n,\mathbf{k}} c^{(a)}_{n,\mathbf{k}} c^{(a)\dagger}_{\bar{n},\mathbf{k}'} c^{(a)}_{\bar{n},\mathbf{k}'}, \\
\bar{V}^{(1)} &= -\frac{3J_z}{4} \sum_{a,n,\mathbf{k},\mathbf{k}'} c^{(a)\dagger}_{n,\mathbf{k}} c^{(a)}_{\bar{n},\mathbf{k}} c^{(\bar{a})\dagger}_{\bar{n},\mathbf{k}'} c^{(\bar{a})}_{n,\mathbf{k}'} \\
&\quad + \frac{3J_z}{4} \sum_{a,n,\mathbf{k},\mathbf{k}'} c^{(a)\dagger}_{n,\mathbf{k}} c^{(a)}_{n,\mathbf{k}} c^{(\bar{a})\dagger}_{\bar{n},\mathbf{k}'} c^{(\bar{a})}_{\bar{n},\mathbf{k}'}, \\
\bar{V}^{(2)} &= -\frac{3J_z}{4} \sum_{a,n,\mathbf{k},\mathbf{k}'} \mathbf{k}\cdot\mathbf{k}' c^{(a)\dagger}_{n,\mathbf{k}} c^{(\bar{a})}_{\bar{n},\mathbf{k}} c^{(\bar{a})\dagger}_{\bar{n},\mathbf{k}'} c^{(a)}_{n,\mathbf{k}'} \\
&\quad + \frac{3J_z}{4} \sum_{a,n,\mathbf{k},\mathbf{k}'} \mathbf{k}\cdot\mathbf{k}' c^{(a)\dagger}_{n,\mathbf{k}} c^{(\bar{a})}_{n,\mathbf{k}} c^{(\bar{a})\dagger}_{\bar{n},\mathbf{k}'} c^{(a)}_{\bar{n},\mathbf{k}'}.
\end{aligned} \tag{A1}
$$

The first two are intravalley interactions, which are only associated with the interactions between different bands at one single valley. The latter two are interactions between different valleys. To investigate the effect of the interaction from the Ising term on the original Dirac cones, we treat these interactions with mean-field approximations [38].

First, we only consider the intravalley interactions. Applying mean-field treatment, the order parameters are chosen as

follows:

$$\chi_{n,s}^{(a)} = \frac{3J_z}{2}\sum_{\mathbf{k}}\left\langle c_{n,\mathbf{k}}^{(a)\dagger} c_{\bar{n},\mathbf{k}}^{(a)}\right\rangle,$$
$$\lambda_{n,s}^{(a)} = \frac{3J_z}{2}\sum_{\mathbf{k}}\left\langle c_{n,\mathbf{k}}^{(a)\dagger} c_{n,\mathbf{k}}^{(a)}\right\rangle,$$
$$\boldsymbol{\chi}_{n,p}^{(a)} = \frac{3J_z}{2}\sum_{\mathbf{k}}\hat{\mathbf{k}}\left\langle c_{n,\mathbf{k}}^{(a)\dagger} c_{\bar{n},\mathbf{k}}^{(a)}\right\rangle,$$
$$\boldsymbol{\lambda}_{n,p}^{(a)} = \frac{3J_z}{2}\sum_{\mathbf{k}}\hat{\mathbf{k}}\left\langle c_{n,\mathbf{k}}^{(a)\dagger} c_{n,\mathbf{k}}^{(a)}\right\rangle. \tag{A2}$$

By definition, $\chi_{n,s}^{(a)*} = \chi_{\bar{n},s}^{(a)}$ and $\boldsymbol{\chi}_{n,p}^{(a)*} = \boldsymbol{\chi}_{\bar{n},p}^{(a)}$. Thus, the mean-field Hamiltonian is given by

$$\begin{aligned}
H_{\mathrm{MF}}^{\mathrm{intra}} = &\sum_{n,\mathbf{k}}\left(nv_F k c_{n,\mathbf{k}}^{(+)\dagger} c_{n,\mathbf{k}}^{(+)} - nv_F k c_{n,\mathbf{k}}^{(-)\dagger} c_{n,\mathbf{k}}^{(-)}\right)\\
&+\frac{1}{2}\sum_{n,a,\mathbf{k}}\left(\lambda_{n,s}^{(a)} c_{\bar{n},\mathbf{k}}^{(a)\dagger} c_{\bar{n},\mathbf{k}}^{(a)} + \lambda_{\bar{n},s}^{(a)*} c_{n,\mathbf{k}}^{(a)\dagger} c_{n,\mathbf{k}}^{(a)}\right)\\
&-\frac{1}{2}\sum_{n,a,\mathbf{k}}\left(\chi_{n,s}^{(a)} c_{\bar{n},\mathbf{k}}^{(a)\dagger} c_{n,\mathbf{k}}^{(a)} + \chi_{n,s}^{(a)*} c_{n,\mathbf{k}}^{(a)\dagger} c_{\bar{n},\mathbf{k}}^{(a)}\right)\\
&+\frac{1}{2}\sum_{n,a,\mathbf{k}}\left(\hat{\mathbf{k}}\cdot\boldsymbol{\lambda}_{n,p}^{(a)} c_{\bar{n},\mathbf{k}}^{(a)\dagger} c_{\bar{n},\mathbf{k}}^{(a)} + \hat{\mathbf{k}}\cdot\boldsymbol{\lambda}_{\bar{n},p}^{(a)} c_{n,\mathbf{k}}^{(a)\dagger} c_{n,\mathbf{k}}^{(a)}\right)\\
&-\frac{1}{2}\sum_{n,a,\mathbf{k}}\left(\hat{\mathbf{k}}\cdot\boldsymbol{\chi}_{\bar{n},p}^{(a)} c_{n,\mathbf{k}}^{(a)\dagger} c_{\bar{n},\mathbf{k}}^{(a)} + \hat{\mathbf{k}}\cdot\boldsymbol{\chi}_{n,p}^{(a)} c_{\bar{n},\mathbf{k}}^{(a)\dagger} c_{n,\mathbf{k}}^{(a)}\right)\\
&+\frac{1}{3J_z}\sum_{n,a}\chi_{n,s}^{(a)}\chi_{\bar{n},s}^{(a)} - \frac{1}{3J_z}\sum_{n,a}\lambda_{n,s}^{(a)}\lambda_{\bar{n},s}^{(a)}\\
&+\frac{1}{3J_z}\sum_{n,a}\boldsymbol{\chi}_{n,p}^{(a)}\cdot\boldsymbol{\chi}_{\bar{n},p}^{(a)} - \frac{1}{3J_z}\sum_{n,a}\boldsymbol{\lambda}_{n,p}^{(a)}\cdot\boldsymbol{\lambda}_{\bar{n},p}^{(a)}.
\end{aligned}\tag{A3}$$

The two valleys in the Hamiltonian above are uncoupled, so we only consider the "+" valley here. For convenience, we ignore the "+" index, and the Hamiltonian reads as

$$\begin{aligned}
H_{\mathrm{MF}}^{\mathrm{intra}} = &\sum_{\mathbf{k},n} v_F k c_{n,\mathbf{k}}^{\dagger} c_{n,\mathbf{k}}\\
&+\sum_{\mathbf{k},n}(\lambda_{n,s} c_{\bar{n},\mathbf{k}}^{\dagger} c_{\bar{n},\mathbf{k}} - \chi_{n,s} c_{\bar{n},\mathbf{k}}^{\dagger} c_{n,\mathbf{k}})\\
&+\sum_{\mathbf{k},n}(\hat{\mathbf{k}}\cdot\boldsymbol{\lambda}_{n,p} c_{\bar{n},\mathbf{k}}^{\dagger} c_{\bar{n},\mathbf{k}} - \hat{\mathbf{k}}\cdot\boldsymbol{\chi}_{n,p} c_{\bar{n},\mathbf{k}}^{\dagger} c_{n,\mathbf{k}})\\
&+\frac{2}{3J_z}\chi_{+,s}\chi_{-,s} - \frac{2}{3J_z}\lambda_{+,s}\lambda_{-,s}\\
&+\frac{2}{3J_z}\boldsymbol{\chi}_{+,p}\cdot\boldsymbol{\chi}_{-,p} - \frac{2}{3J_z}\boldsymbol{\lambda}_{+,p}\cdot\boldsymbol{\lambda}_{-,p}.
\end{aligned}\tag{A4}$$

Choose a gauge to constrain the order parameters to be real and we get the "+" valley Hamiltonian,

$$\begin{aligned}
&H_{\mathrm{MF}}^{\mathrm{intra}}\\
&= \sum_{\mathbf{k}}\psi_{\mathbf{k}}^{\dagger}\begin{pmatrix} v_F k + \lambda_{-,s} & -\chi_s - \frac{1}{\sqrt{2}}\chi_p e^{-i\theta_k}\\ -\chi_s - \frac{1}{\sqrt{2}}\chi_p e^{i\theta_k} & -v_F k + \lambda_{+,s}\end{pmatrix}\psi_{\mathbf{k}}\\
&\quad+\frac{2}{3J_z}\chi_s^2 - \frac{2}{3J_z}\lambda_{+,s}\lambda_{-,s} + \frac{2}{3J_z}\chi_p^2,
\end{aligned}\tag{A5}$$

where $\psi_{\mathbf{k}} = (c_{+,\mathbf{k}} \quad c_{-,\mathbf{k}})^{\mathrm{T}}$, χ_p is the amplitude of p-wave excitonic order, and we have used $\chi_{+,s} = \chi_{-,s} := \chi_s$, $\boldsymbol{\chi}_{-,p} = \boldsymbol{\chi}_{+,p}^{*}$. The $\hat{\mathbf{k}}\cdot\boldsymbol{\lambda}_{-,p}$ term does not satisfy the Hermitian condition, so it is discarded. The ground-state energy is obtained to be

$$\begin{aligned}
E_G = &-\sum_{\mathbf{k}}\left\{\lambda_1 + \left[\frac{1}{2}\chi_p^2 + \sqrt{2}\chi_p\chi_s\cos\theta\right.\right.\\
&\left.\left.+\chi_s^2 + (\lambda_2 + v_F k)^2\right]\right\}\\
&+\frac{2}{3J_z}\chi_s^2 - \frac{2}{3J_z}\left(\lambda_1^2 - \lambda_2^2\right) + \frac{2}{3J_z}\chi_p^2,
\end{aligned}\tag{A6}$$

where we have defined $\lambda_1 = \frac{1}{2}(\lambda_{+,s} + \lambda_{-s})$, $\lambda_2 = \frac{1}{2}(\lambda_{+,s} - \lambda_{-s})$.

Only λ_2, χ_p, and χ_s determine the ground state energy in a nontrivial way, while λ_1 just shifts the ground state energy by a constant term. Taking the continuum limit, we get their self-consistent equations,

$$\begin{aligned}
\lambda_2 &= \frac{3J_z}{8}\int\frac{kdk}{2\pi}\int_0^{2\pi}\frac{d\theta}{2\pi}\frac{\lambda_2 + v_F k}{\sqrt{A}},\\
\chi_p &= \frac{3J_z}{8}\int\frac{kdk}{2\pi}\int_0^{2\pi}\frac{d\theta}{2\pi}\frac{\chi_p + \sqrt{2}\chi_s\cos\theta}{\sqrt{A}},\\
\chi_s &= \frac{3J_z}{8}\int\frac{kdk}{2\pi}\int_0^{2\pi}\frac{d\theta}{2\pi}\frac{2\chi_s + \sqrt{2}\chi_p\cos\theta}{\sqrt{A}},
\end{aligned}\tag{A7}$$

where $A = \chi_p^2/2 + \sqrt{2}\chi_p\chi_s\cos\theta + \chi_s^2 + (\lambda_2 + v_F k)^2$. Rescale these equations by substituting $\lambda_2 = \lambda_2' v_F\Lambda$, $\chi_p = \chi_p' v_F\Lambda$, $\chi_s = \chi_s' v_F\Lambda$, $J_z = J' v_F\Lambda$, $k = k'\Lambda$, we get

$$\begin{aligned}
\lambda_2' &= \frac{3J'}{32\pi^2}\int k'dk'\int_0^{2\pi}d\theta\frac{\lambda_2' + k'}{\sqrt{A'}},\\
\chi_p' &= \frac{3J'}{32\pi^2}\int k'dk'\int_0^{2\pi}d\theta\frac{\chi_p' + \sqrt{2}\chi_s'\cos\theta}{\sqrt{A'}},\\
\chi_s' &= \frac{3J'}{32\pi^2}\int k'dk'\int_0^{2\pi}d\theta\frac{2\chi_s' + \sqrt{2}\chi_p'\cos\theta}{\sqrt{A'}},
\end{aligned}\tag{A8}$$

where $A' = \chi_p'^2/2 + \sqrt{2}\chi_p'\chi_s'\cos\theta + \chi_s'^2 + (\lambda_2' + k')^2$.

As shown in the main text, after self-consistency calculations, we find that only s-wave excitonic orders dominate, so we will only consider this order in the following discussions.

Now consider the inter-valley interactions. After applying the mean-field approximation, we have

$$\begin{aligned} H_{MF}^{\text{inter}} =& -\frac{1}{2}\sum_{\mathbf{k},n,a}\left(\chi_{n,s}^{(a)}c_{\bar{n},\mathbf{k}}^{(\bar{a})\dagger}c_{n,\mathbf{k}}^{(\bar{a})}+\chi_{\bar{n},s}^{(\bar{a})}c_{n,\mathbf{k}}^{(a)\dagger}c_{\bar{n},\mathbf{k}}^{(a)}\right)\\ &+\frac{1}{2}\sum_{\mathbf{k},n,a}\left(\lambda_{n,s}^{(a)}c_{\bar{n},\mathbf{k}}^{(\bar{a})\dagger}c_{\bar{n},\mathbf{k}}^{(\bar{a})}+\lambda_{\bar{n},s}^{(\bar{a})}c_{n,\mathbf{k}}^{(a)\dagger}c_{n,\mathbf{k}}^{(a)}\right)\\ &-\frac{1}{2}\sum_{\mathbf{k},n,a}\hat{\mathbf{k}}\cdot\left(\bar{\boldsymbol{\chi}}_{n,p}^{(a)}c_{\bar{n},\mathbf{k}}^{(\bar{a})\dagger}c_{n,\mathbf{k}}^{(a)}+\bar{\boldsymbol{\chi}}_{\bar{n},p}^{(\bar{a})}c_{n,\mathbf{k}}^{(a)\dagger}c_{\bar{n},\mathbf{k}}^{(\bar{a})}\right)\\ &+\frac{1}{2}\sum_{\mathbf{k},n,a}\hat{\mathbf{k}}\cdot\left(\boldsymbol{\xi}_{n,p}^{(a)}c_{\bar{n},\mathbf{k}}^{(\bar{a})\dagger}c_{\bar{n},\mathbf{k}}^{(a)}+\boldsymbol{\xi}_{\bar{n},p}^{(\bar{a})}c_{n,\mathbf{k}}^{(a)\dagger}c_{n,\mathbf{k}}^{(\bar{a})}\right)\\ &-\frac{1}{3J_z}\sum_{a,n}\left(\boldsymbol{\xi}_{n,p}^{(a)}\cdot\boldsymbol{\xi}_{\bar{n},p}^{(\bar{a})}-\bar{\boldsymbol{\chi}}_{n,p}^{(a)}\cdot\bar{\boldsymbol{\chi}}_{\bar{n},p}^{(\bar{a})}\right)\\ &-\frac{1}{3J_z}\sum_{a,n}\left(\lambda_{n,s}^{(a)}\lambda_{\bar{n},s}^{(\bar{a})}-\chi_{n,s}^{(a)}\chi_{\bar{n},s}^{(\bar{a})}\right), \end{aligned} \tag{A9}$$

where the newly decoupled order parameters are defined as follows:

$$\bar{\boldsymbol{\chi}}_{n,p}^{(a)}=\frac{3J_z}{2}\sum_{\mathbf{k}}\hat{\mathbf{k}}\left\langle c_{n,\mathbf{k}}^{(a)\dagger}c_{\bar{n},\mathbf{k}}^{(\bar{a})}\right\rangle, \tag{A10}$$

$$\boldsymbol{\xi}_{n,p}^{(a)}=\frac{3J_z}{2}\sum_{\mathbf{k}}\hat{\mathbf{k}}\left\langle c_{n,\mathbf{k}}^{(a)\dagger}c_{\bar{n},\mathbf{k}}^{(\bar{a})}\right\rangle. \tag{A11}$$

$\bar{\boldsymbol{\chi}}_{n,p}^{(a)}$ is the intervalley p-wave excitonic order. We only consider the excitonic orders since only the excitonic orders are relevant to the original spin picture. After adding the excitonic orders from the intravalley interactions to the Hamiltonian, we arrive at a simplified Hamiltonian containing all Ising terms

$$H_{\text{MF}}=\sum_{\mathbf{k}}\Psi_{\mathbf{k}}^{\dagger}\mathcal{H}\Psi_{\mathbf{k}}+\frac{2}{3J_z}(\chi_s^{(+)}+\chi_s^{(-)})^2+\frac{4}{3J_z}\bar{\boldsymbol{\chi}}_p^{(+)}\cdot\bar{\boldsymbol{\chi}}_p^{(-)}, \tag{A12}$$

with $\Psi_{\mathbf{k}}=(c_{+,\mathbf{k}}^{(+)}\quad c_{-,\mathbf{k}}^{(+)}\quad c_{+,\mathbf{k}}^{(-)}\quad c_{-,\mathbf{k}}^{(-)})^{\text{T}}$, and

$$\mathcal{H}=\begin{pmatrix} v_Fk & -\sum_a\chi_s^{(a)} & 0 & -\bar{\boldsymbol{\chi}}_p^{(+)}\cdot\hat{\mathbf{k}}\\ -\sum_a\chi_s^{(a)} & -v_Fk & -\bar{\boldsymbol{\chi}}_p^{(+)}\cdot\hat{\mathbf{k}} & 0\\ 0 & -\bar{\boldsymbol{\chi}}_p^{(-)}\cdot\hat{\mathbf{k}} & -v_Fk & \sum_a\chi_s^{(a)}\\ -\bar{\boldsymbol{\chi}}_p^{(-)}\cdot\hat{\mathbf{k}} & 0 & \sum_a\chi_s^{(a)} & v_Fk \end{pmatrix}, \tag{A13}$$

where we have used $\chi_{\pm,s}^{(a)}=\chi_s^{(a)}$, $\bar{\boldsymbol{\chi}}_{\pm,p}^{(a)}=\bar{\boldsymbol{\chi}}_p^{(a)}$. Thus, we obtain the effective Hamiltonian which contains the XY term and the Ising term.

[1] P. W. Anderson, Phys. Rev. **79**, 350 (1950).
[2] S. Sachdev, Nat. Phys. **4**, 173 (2008).
[3] L. Balents, Nature (London) **464**, 199 (2010).
[4] L. Savary and L. Balents, Rep. Prog. Phys. **80**, 016502 (2017).
[5] Y. Zhou, K. Kanoda, and T.-K. Ng, Rev. Mod. Phys. **89**, 025003 (2017).
[6] M. R. Norman, Rev. Mod. Phys. **88**, 041002 (2016).
[7] A. Banerjee, J. Yan, J. Knolle, C. A. Bridges, M. B. Stone, M. D. Lumsden, D. G. Mandrus, D. A. Tennant, R. Moessner, and S. E. Nagler, Science **356**, 1055 (2017).
[8] K. v. Klitzing, G. Dorda, and M. Pepper, Phys. Rev. Lett. **45**, 494 (1980).
[9] D. C. Tsui, H. L. Stormer, and A. C. Gossard, Phys. Rev. Lett. **48**, 1559 (1982).
[10] R. B. Laughlin, Phys. Rev. Lett. **50**, 1395 (1983).
[11] F. D. M. Haldane, Phys. Rev. Lett. **51**, 605 (1983).
[12] J. G. Bednorz and K. A. Müller, Z. Phys. B **64**, 189 (1986).
[13] P. A. Lee, N. Nagaosa, and X.-G. Wen, Rev. Mod. Phys. **78**, 17 (2006).
[14] S. Sachdev, *Quantum Phase Transitions* (Cambridge University Press, Cambridge, 2000)
[15] S. R. White, Phys. Rev. Lett. **69**, 2863 (1992).
[16] U. Schollwöck, Ann. Phys. **326**, 96 (2011).
[17] M. Levin and C. P. Nave, Phys. Rev. Lett. **99**, 120601 (2007).
[18] A. Auerbach, *Interacting Electrons and Quantum Magnetism* (Springer, New York, 2012).
[19] D. Yoshioka, *Strong Correlation and Superconductivity* (Springer, Berlin, 1989), pp. 124–131.
[20] X.-G. Wen, Phys. Rev. B **65**, 165113 (2002).
[21] X.-Y. Song, C. Wang, A. Vishwanath, and Y.-C. He, Nat. Commun. **10**, 1 (2019).
[22] M. Hermele, T. Senthil, and M. P. A. Fisher, Phys. Rev. B **72**, 104404 (2005).
[23] B. I. Halperin, P. A. Lee, and N. Read, Phys. Rev. B **47**, 7312 (1993).
[24] J. K. Jain, Phys. Rev. Lett. **63**, 199 (1989).
[25] A. Lopez, A. G. Rojo, and E. Fradkin, Phys. Rev. B **49**, 15139 (1994).
[26] S. Maiti and T. Sedrakyan, Phys. Rev. B **99**, 174418 (2019).
[27] S. Maiti and T. A. Sedrakyan, Phys. Rev. B **100**, 125428 (2019).
[28] T. A. Sedrakyan, L. I. Glazman, and A. Kamenev, Phys. Rev. B **89**, 201112(R) (2014).
[29] T. Sedrakyan, R. Moessner, and A. Kamenev, Phys. Rev. B **102**, 024430 (2020).
[30] A. Altland and B. D. Simons, *Condensed Matter Field Theory*, 2nd ed. (Cambridge University Press, Cambridge, 2010).

[31] G. V. Dunne, in *Aspects topologiques de la physique en basse dimension. Topological aspects of low dimensional systems*, edited by A. Comtet, T. Jolicœur, S. Ouvry, and F. David (Springer Berlin Heidelberg, Berlin, Heidelberg, 1999) pp. 177–263.
[32] T. A. Sedrakyan, V. M. Galitski, and A. Kamenev, Phys. Rev. B **95**, 094511 (2017).
[33] R. Wang, B. Wang, and T. Sedrakyan, Phys. Rev. B **105**, 054404 (2022).
[34] K. Yang, L. K. Warman, and S. M. Girvin, Phys. Rev. Lett. **70**, 2641 (1993).
[35] R. Wang, Z. Y. Xie, B. Wang, and T. Sedrakyan, Phys. Rev. B **106**, L121117 (2022).
[36] R. Wang, B. Wang, and T. A. Sedrakyan, Phys. Rev. B **98**, 064402 (2018).
[37] O. Türker and K. Yang, Phys. Rev. B **105**, 155150 (2022).
[38] H. Wei, S.-P. Chao, and V. Aji, Phys. Rev. Lett. **109**, 196403 (2012).
[39] R. Wang, O. Erten, B. Wang, and D. Xing, Nat. Commun. **10**, 210 (2019).
[40] E. H. Lieb, Phys. Rev. Lett. **73**, 2158 (1994).
[41] S.-C. Zhang, Science **275**, 1089 (1997).
[42] E. Demler, W. Hanke, and S.-C. Zhang, Rev. Mod. Phys. **76**, 909 (2004).
[43] A. M. Tsvelik, *Quantum Field Theory in Condensed Matter Physics*, 2nd ed. (Cambridge University Press, Cambridge, 2003).
[44] P. Zanardi and N. Paunković, Phys. Rev. E **74**, 031123 (2006).
[45] P. Buonsante and A. Vezzani, Phys. Rev. Lett. **98**, 110601 (2007).
[46] S.-J. Gu, Int. J. Mod. Phys. B **24**, 4371 (2010).
[47] A. F. Albuquerque, F. Alet, C. Sire, and S. Capponi, Phys. Rev. B **81**, 064418 (2010).
[48] Z. Zhu, G. Sun, W.-L. You, and D.-N. Shi, Phys. Rev. A **98**, 023607 (2018).
[49] G. Sun, Phys. Rev. A **96**, 043621 (2017).
[50] G. Sun, A. K. Kolezhuk, and T. Vekua, Phys. Rev. B **91**, 014418 (2015).
[51] B.-B. Wei, Phys. Rev. A **99**, 042117 (2019).
[52] T. Lv, T.-C. Yi, L. Li, G. Sun, and W.-L. You, Phys. Rev. A **105**, 013315 (2022).
[53] G. Sun, B.-B. Wei, and S.-P. Kou, Phys. Rev. B **100**, 064427 (2019).
[54] G. Sun, J.-C. Tang, and S.-P. Kou, Front. Phys. **17**, 33502 (2022).
[55] Y.-C. Tzeng, C.-Y. Ju, G.-Y. Chen, and W.-M. Huang, Phys. Rev. Res. **3**, 013015 (2021).
[56] D. Schwandt, F. Alet, and S. Capponi, Phys. Rev. Lett. **103**, 170501 (2009).
[57] W.-L. You and Y.-L. Dong, Phys. Rev. B **84**, 174426 (2011).
[58] S.-J. Gu, H.-M. Kwok, W.-Q. Ning, and H.-Q. Lin, Phys. Rev. B **77**, 245109 (2008).
[59] W.-C. Yu, H.-M. Kwok, J. Cao, and S.-J. Gu, Phys. Rev. E **80**, 021108 (2009).
[60] N. Paunković, P. D. Sacramento, P. Nogueira, V. R. Vieira, and V. K. Dugaev, Phys. Rev. A **77**, 052302 (2008).
[61] J. Ma, L. Xu, H.-N. Xiong, and X. Wang, Phys. Rev. E **78**, 051126 (2008).
[62] H.-M. Kwok, C.-S. Ho, and S.-J. Gu, Phys. Rev. A **78**, 062302 (2008).